





What are “X-shaped” Radio Sources Telling Us? I. Very Large Array Imaging of a Large Sample of Candidate XRGs

David H. Roberts¹ , Lakshmi Saripalli², Kevin X. Wang¹, Mayuri Sathyanarayana Rao², Ravi Subrahmanyan² , Carly C. KleinStern¹, Christopher Y. Morii-Sciolla¹, and Liana Simpson¹

¹Department of Physics, MS-057, Brandeis University, Waltham, MA 02453-0911, USA; roberts@brandeis.edu

²Raman Research Institute, C. V. Raman Avenue, Sadashivanagar, Bangalore 560080, India; lsaripal@rri.res.in

Received 2017 August 4; revised 2017 October 13; accepted 2017 October 27; published 2018 January 5

Abstract

We present archival and Jansky Very Large Array multi-frequency multi-array radio continuum imaging of a unique sample of 100 radio sources that have been selected to be candidate “X-shaped” radio galaxies (XRGs). The archival data were calibrated in AIPS and imaged using DIFMAP, while the new Very Large Array data were calibrated and imaged in CASA. No attempt was made to re-image the archival data in CASA. Altogether we present images of 95 of the 100 sources. These observations give us the opportunity to study radio sources with synchrotron plasma that is significantly offset from the main radio axis and therefore to open a window into investigations of physical mechanisms responsible for depositing the plasma in off-axis regions. Here, we present the technical details of the observations and all of the total intensity images, while in subsequent papers we use them to examine critically various models for the formation of XRGs. Spectral index and linear polarization information is also presented and analyzed in further papers in this series.

Key words: galaxies: active – galaxies: nuclei – radio continuum: galaxies

Supporting material: figure sets, machine-readable tables

1. Introduction

1.1. Characteristics of X-shaped Radio Galaxies (XRGs)

XRGs (also called “winged radio galaxies”)³ are a small (~7%) subclass of extragalactic radio sources that in addition to the usual pair of extended lobes contain a second pair of lower surface brightness wings of emission (Leahy & Parma 1992). This leads to an “X” shaped appearance. Thus, a defining characteristic is the presence of synchrotron plasma off the main axis of the source. For reasons discussed below, these structures may hold clues about the nature of the central engines.

1.2. Goals of This Paper

There is no universally accepted explanation for the origin of XRG structures. One possibility is that the wings are the result of backflow from the main lobes that is deflected by the galactic halo in an inversion-symmetric manner (Leahy & Williams 1984). There are difficulties with this explanation (e.g., how can the wings in some XRGs be longer than the lobes?; Dennett-Thorpe et al. 2002). Another explanation is that the axis of the underlying active galactic nucleus (AGN) has flipped, perhaps due to the interaction of the supermassive black hole (SMBH) with a second SMBH (Merritt & Ekers 2002); such SMBH pairs are presumed to be the natural results of galaxy mergers (Begelman et al. 1980). Because the coalescence of binary SMBH systems is thought to be the primary source of the low-frequency gravitational-wave background (Shannon et al. 2013, 2015), the rate of occurrence of XRGs can give us a handle on the frequency of SMBH mergers (Merritt & Ekers 2002; Roberts et al. 2015b). A more complete introduction to XRGs is given in Saripalli & Roberts (2017).

Cheung (2007) had previously set out to greatly expand the number of XRGs by systematically searching for candidate sources to be observed in greater detail in follow-up programs (see Section 2 below for the selection criteria). In our earlier work on this sample (Roberts et al. 2015a), we made archival Very Large Array (VLA) images of 52 of the sources. We divided the XRG candidates into two classes: those with deviations from a linear structure at the inner edges of the lobes and those with deviations at the outer edges of the lobes. We also defined a class of “true XRGs” to be those with a second swath of emission crossing the core and disconnected from the main lobes. In Roberts et al. (2015b), we used these data to address the rate of formation of system with binary SMBHs. The reader is referred to those two papers for further details.

To better understand this unique population of radio galaxies we embarked on a project to image the entire sample of candidate XRGs compiled by Cheung (2007). We observed the sample using the Karl G. Jansky VLA in a multi-frequency, multi-array set of observations in total intensity and polarization. In this paper, the first in a series, we present our entire set of images and give full observational details. We observed 86 radio galaxies and quasars out of this sample (the rest were missed due to insufficient observing time). Including the archival images of 52 sources presented in Roberts et al. (2015a), we made images of 95/100 of the Cheung candidate XRGs. In our companion paper (Saripalli & Roberts 2017), we make use of these images to characterize the sources imaged, presenting a thorough analysis of how the structures may have formed and what the implications are to the existing models.

The structure of this paper is as follows. Section 2 describes the sample selection process, Section 3 has the details of the observations and imaging methods, Section 4 presents the images, and Section 5 summarizes the paper.

³ Although a small fraction of these sources are quasars, we will continue to refer to the whole class as XRGs.

Table 1
The Cheung Sample of X-shaped Radio Source Candidates^a

Source	R.A.	Decl.	z^b
J0001–0033	00:01:40.2	–00:33:50.6	0.247
J0033–0149	00:33:02.4	–01:49:56.6	0.1301
J0036+0048	00:36:36.2	+00:48:53.4	0.591
J0045+0021	00:45:42.1	+00:21:05.5	0.433*
J0049+0059	00:49:39.4	+00:59:53.8	0.3044
J0113+0106	01:13:41.1	+01:06:08.5	0.281
J0115–0000	01:15:27.4	–00:00:01.5	0.381
J0143–0119	01:43:16.8	–01:19:00.8	0.520
J0144–0830	01:44:10.0	–08:30:02.8	0.181
J0145–0159	01:45:20.0	–01:59:47.9	0.1264
J0147–0851	01:47:19.3	–08:51:19.6	0.455
J0211–0920	02:11:47.0	–09:20:36.6	0.236*
J0225–0738	02:25:08.6	–07:38:49.1	0.659
J0702+5002	07:02:47.9	+50:02:05.3	0.0946
J0725+5835	07:25:32.3	+58:35:27.4	NA
J0805+4854	08:05:44	+48:54:58	NA
J0813+4347	08:13:00.1	+43:47:48.5	0.128
J0821+2922	08:21:49.6	+29:22:44.4	0.313*
J0836+3125	08:36:35.5	+31:25:51.2	0.376
J0838+3253	08:38:44.6	+32:53:11.8	0.213
J0845+4031	08:45:08.4	+40:31:15.4	0.429
J0846+3956	08:46:03.6	+39:56:57.9	0.257*
J0859–0433	08:59:50.2	–04:33:06.9	0.356
J0914+1715	09:14:05.2	+17:15:54.3	0.52
J0917+0523	09:17:44.3	+05:23:10.1	0.592
J0924+4233	09:24:47.0	+42:33:47.1	0.227
J0941–0143	09:41:22.6	–01:43:01.1	0.383
J0941+2147	09:41:58.3	+21:47:44.2	0.572*
J0943+2834	09:43:02.2	+28:34:45.8	0.574
J1005+1154	10:05:52.5	+11:54:37	0.166
J1008+0030	10:08:11.4	+00:30:00	0.0977
J1015+5944	10:15:41.1	+59:44:45.2	0.527
J1040+5056	10:40:22.5	+50:56:25.1	0.154
J1043+3131	10:43:18.6	+31:31:06.1	0.036
J1049+4422	10:49:35.3	+44:22:04	0.477*
J1054+5521	10:54:00.6	+55:21:53	NA
J1055–0707	10:55:52.6	–07:07:19.1	NA
J1102+0250	11:02:06.6	+02:50:45.7	NA
J1111+4050	11:11:39.7	+40:50:24.1	0.0737
J1114+2632	11:14:27.1	+26:32:58.8	0.66*
J1120+4354	11:20:16.2	+43:54:51.4	0.612
J1128+1919	11:28:37.7	+19:19:57	0.21
J1135–0737	11:35:36.8	–07:37:00.1	0.602
J1140+1057	11:40:49.7	+10:57:56.3	0.081
J1200+6105	12:00:06	+61:05:44.5	0.294*
J1201–0703	12:01:25.8	–07:03:11	NA
J1202+4915	12:02:35.1	+49:15:31.7	0.688*
J1206+3812	12:06:17.4	+38:12:34.9	0.838
J1207+3352	12:07:32.9	+33:52:40.1	0.079
J1210–0341	12:10:18.8	–03:41:53.3	0.1963
J1210+1121	12:10:12.0	+11:21:02.7	0.178
J1211+4539	12:11:02.5	+45:39:14.4	0.698*
J1218+1955	12:18:59.2	+19:55:28	0.424
J1227–0742	12:27:12.5	–07:42:00	0.459
J1227+2155	12:27:49.4	+21:55:19.6	NA
J1228+2642	12:28:03.8	+26:42:26.7	0.201
J1232–0717	12:32:52.5	–07:17:28.9	NA
J1247+4646	12:47:26.8	+46:46:06	0.838*
J1253+3435	12:53:24.3	+34:35:18.2	0.358
J1258+3227	12:58:32.9	+32:27:40.8	NA
J1309–0012	13:09:49.7	–00:12:35.6	0.419
J1310+5458	13:10:15.4	+54:58:34.2	0.355
J1316+2427	13:16:38.3	+24:27:32.4	0.447
J1327–0203	13:27:38.2	–02:03:9.9	0.183
J1330–0206	13:30:10.3	–02:06:18	0.0866
J1339–0016	13:39:34.2	–00:16:35.5	0.1452
J1342+2547	13:42:45.3	+25:47:11.5	0.585
J1345+5233	13:45:41.6	+52:33:35.6	0.4*
J1348+4411	13:48:04.6	+44:11:24.2	0.266
J1351+5559	13:51:42.1	+55:59:43.1	0.069
J1353+0724	13:53:06.4	+07:24:37.1	0.316*
J1406–0154	14:06:48.6	–01:54:16.5	0.64

Table 1
(Continued)

Source	R.A.	Decl.	z^b
J1406+0657	14:06:02.4	+06:57:15.7	0.549
J1408+0225	14:08:28.4	+02:25:50.3	0.179
J1411+0907	14:11:21.1	+09:07:35.4	0.194*
J1424+2637	14:24:40.5	+26:37:30.5	0.037
J1430+5217	14:30:17.3	+52:17:35	0.368
J1433+0037	14:33:51.9	+00:37:23.4	0.504
J1434+5906	14:34:02.2	+59:06:53.3	0.538
J1437+0834	14:37:38.9	+08:34:22.1	0.316*
J1444+4147	14:44:07.2	+41:47:50.3	0.188
J1454+2732	14:54:42.2	+27:32:11.8	0.692*
J1455+3237	14:55:58.3	+32:37:32.5	0.084
J1456+2542	14:56:43.2	+25:42:17.5	0.536
J1459+2903	14:59:41.9	+29:03:31.8	0.146
J1501+0752	15:01:57.4	+07:52:26.7	0.659
J1515–0532	15:15:33.7	–05:32:51	NA
J1522+4527	15:22:13.1	+45:27:57	0.45*
J1537+2648	15:37:07.3	+26:48:23.2	0.287
J1600+2058	16:00:39.0	+20:58:51.7	0.174
J1603+5242	16:03:45.0	+52:42:20.6	0.292
J1606+0000	16:06:12.7	+00:00:27.1	0.059
J1606+4517	16:06:38.9	+45:17:37.1	0.556
J1614+2817	16:14:28.4	+28:17:31	0.107
J1625+2705	16:25:30.7	+27:5:46.3	0.525
J1653+3115	16:53:37.3	+31:15:27.5	0.652
J1655+4551	16:55:16.2	+45:51:08	0.478*
J1656+3952	16:56:36.6	+39:52:58.3	0.3
J2226+0125	22:26:45.6	+01:25:11	0.216*
J2359–1041	23:59:46.5	–10:41:15.4	0.216*

Notes.^a Cheung (2007).^b Redshifts are largely from SDSS DR-12, with the remaining ones from Cheung (2007), Cheung et al. (2009), and Landt et al. (2010). An * is for photometric redshifts from SDSS DR-12, while NA indicates that no redshift information is available.

(This table is available in machine-readable form.)

Table 2
Log of Very Large Array Observations of the
Cheung Sample of Candidate XRGs

Source	Archival ^a Band/Array	JVLA Band/Array, Date
J0001–0033	L/A	S/C, 2016 Feb 07; S/B, 2016 May 30; L/B, 2016 Jun 03
J0033–0149	...	S/C, 2016 Feb 07; S/B, 2016 May 30; L/B, 2016 Jun 03
J0036+0048	...	S/C, 2016 Feb 07; S/B, 2016 May 30; L/B, 2016 Jun 03
J0045+0021	L/A; C/B	S/C, 2016 Feb 07; S/B, 2016 May 30; L/B, 2016 Jun 03
J0049+0059	L/A	S/C, 2016 Feb 07; S/B, 2016 May 30; L/B, 2016 Jun 03
J0113+0106	L/A; C/B	S/C, 2016 Feb 07; S/B, 2016 May 30; L/B, 2016 Jun 03
J0115–0000	...	S/C, 2016 Feb 07; S/B, 2016 May 30; L/B, 2016 Jun 03
J0143–0119	L/A; C/B	S/C, 2016 Feb 04; S/B, 2016 May 30; L/B, 2016 May 31
J0144–0830	L/A	S/C, 2016 Feb 04; S/B, 2016 May 30; L/B, 2016 May 31
J0145–0159	L/A	S/C, 2016 Feb 04; S/B, 2016 May 30; L/B, 2016 May 31
J0147–0851	...	S/C, 2016 Feb 04; S/B, 2016 May 30; L/B, 2016 May 31
J0211–0920	L/A	S/C, 2016 Feb 04; S/B, 2016 May 30; L/B, 2016 May 31
J0225–0738	...	S/C, 2016 Feb 04; S/B, 2016 May 30

Table 2
(Continued)

Source	Archival ^a Band/Array	JVLA Band/Array, Date
J0702+5002	L/A	S/C, 2016 Feb 04; S/B, 2016 May 28; L/B, 2016 May 29
J0725+5835	...	S/C, 2016 Feb 04; S/B, 2016 May 28; L/B, 2016 May 29
J0805+4854	...	S/C, 2016 Feb 04; S/B, 2016 May 28; L/B, 2016 May 29
J0813+4347	L/A	S/C, 2016 Feb 04; S/B, 2016 May 28; L/B, 2016 May 29; L/A, 2016 Dec 27
J0821+2922	L/A	S/C, 2016 Feb 04; S/B, 2016 May 22; L/B, 2016 May 28; L/A, 2017 Jan 10
J0836+3125	...	S/C, 2016 Feb 04; S/B, 2016 May 22; L/B, 2016 May 28
J0838+3253	...	S/C, 2016 Feb 04; S/B, 2016 May 22; L/B, 2016 May 28; L/A, 2017 Jan 10
J0845+4031	L/A	S/C, 2016 Feb 04; S/B, 2016 May 22; L/B, 2016 May 28; L/A, 2016 Dec 27
J0846+3956	L/A	S/C, 2016 Feb 04; S/B, 2016 May 22; L/B, 2016 May 28
J0859-0433	L/A	S/B, 2016 Jun 03; L/B, 2016 Aug 14
J0914+1715	...	S/C, 2016 Feb 04; L/B, 2016 May 30; S/B, 2016 Jun 19; L/A, 2017 Jan 10
J0917+0523	L/A	S/B, 2016 Jun 03; L/B, 2016 Aug 14; L/A, 2017 Jan 10
J0924+4233	L/A	S/C, 2016 Apr 22; S/B, 2016 May 22; L/B, 2016 May 28
J0941-0143	L/A	S/B, 2016 Jun 03; L/B, 2016 Aug 14
J0941+2147	...	S/C, 2016 Feb 04; L/B, 2016 May 30; S/B, 2016 Jun 19; L/A, 2017 Jan 10
J0943+2834	...	S/C, 2016 Feb 04; L/B, 2016 May 30; S/B, 2016 Jun 19; L/A, 2017 Jan 10
J1005+1154	L/A	S/B, 2016 Jun 03; L/B, 2016 Aug 14; L/A, 2017 Jan 10
J1008+0030	L/A	S/B, 2016 Jun 03; L/B, 2016 Aug 14; L/A, 2017 Jan 10
J1015+5944	L/A	S/C, 2016 Apr 22; S/B, 2016 Jul 16
J1040+5056	...	S/C, 2016 Apr 22; S/B, 2016 Jul 16
J1043+3131	L/A; C/B	S/C, 2016 Apr 22; S/B, 2016 Jul 16
J1049+4422	...	S/C, 2016 Apr 22; S/B, 2016 Jul 16
J1054+5521	L/A	S/C, 2016 Apr 22; S/B, 2016 Jul 16
J1055-0707	...	S/C, 2016 Mar 29; S/B 2016 Jul 24;
J1102+0250	...	S/C, 2016 Mar 29; S/B, 2016 Jul 24
J1111+4050	L/A; C/B	...
J1114+2632	...	S/C, 2016 Apr 22; S/B, 2016 Jul 16
J1120+4354	...	S/C, 2016 Apr 22; S/B, 2016 Jul 16; L/B, 2016 Aug 26
J1128+1919	...	S/B, 2016 Jun 15; L/B, 2016 Aug 26
J1135-0737	L/A	S/C, 2016 Mar 29; S/B, 2016 Jul 24
J1140+1057	...	S/B, 2016 Jun 15; L/B, 2016 Aug 26
J1200+6105	...	S/B, 2016 May 22; S/B, 2016 Jun 25
J1201-0703	...	S/C, 2016 Mar 29; S/B, 2016 Jul 24
J1202+4915	L/A	S/B, 2016 Jun 25
J1206+3812	L/A; C/B	S/B, 2016 Jul 22
J1207+3352	L/A; C/B	S/B, 2016 Jul 22
J1210-0341	L/A	S/C, 2016 Mar 29; S/B, 2016 Jul 24
J1210+1121	...	S/B, 2016 Jun 15
J1211+4539	L/A	...
J1218+1955	...	S/B, 2016 Jul 22
J1227-0742	L/A	S/C, 2016 Mar 29; S/B, 2016 Jul 24
J1227+2155	L/A	S/C, 2016 Mar 29; S/B, 2016 Jul 22
J1228+2642	L/A	S/B, 2016 Jul 22
J1232-0717	...	S/C, 2016 Mar 29; S/B, 2016 Jul 24
J1247+4646	...	S/B, 2016 Jun 25
J1253+3435	L/A	S/B, 2016 Jul 22
J1258+3227	...	S/B, 2016 Jul 22
J1309-0012	C/B	S/B, 2016 Jul 24
J1310+5458	L/A	S/B, 2016 Jun 25
J1316+2427	...	S/B, 2016 Jul 24
J1327-0203	L/A	S/B, 2016 Jul 24
J1330-0206	...	S/B, 2016 Jul 24

Table 2
(Continued)

Source	Archival ^a Band/Array	JVLA Band/Array, Date
J1339-0016	...	S/B, 2016 Jul 24
J1342+2547	L/A	S/B, 2016 Jul 24
J1345+5233	L/A	S/C, 2016 Mar 30; S/AB, 2016 Sep 25
J1348+4411	L/A	S/C, 2016 Mar 30; S/AB, 2016 Sep 25
J1351+5559	...	S/C, 2016 Mar 30; S/AB, 2016 Sep 25
J1353+0724
J1406-0154	L/A	S/B, 2016 Jul 24
J1406+0657	L/A	...
J1408+0225	L/A	...
J1411+0907
J1424+2637	...	S/B, 2016 Jul 24
J1430+5217	L/A	S/C, 2016 Mar 30; S/AB, 2016 Sep 25
J1433+0037
J1434+5906	L/A	S/C, 2016 Mar 30; S/AB, 2016 Sep 25
J1437+0834
J1444+4147	...	S/C, 2016 Mar 30
J1454+2732
J1455+3237	...	S/B, 2016 Jul 24
J1456+2542	L/A	...
J1459+2903	L/A; C/B	...
J1501+0752	...	S/B, 2016 Aug 05
J1515+0532	...	S/B, 2016 Aug 05
J1522+4527	...	S/C, 2016 Mar 30
J1537+2648	...	S/C, 2016 Mar 30; S/B, 2016 Aug 05
J1600+2058	L/A	S/C, 2016 Mar 30; S/B, 2016 Aug 05
J1603+5242	...	S/C, 2016 Mar 30
J1606+0000	L/A	S/B, 2016 Aug 05
J1606+4517	L/A	S/C, 2016 Mar 30
J1614+2817	L/A	S/B, 2016 Aug 05
J1625+2705	L/A	S/B, 2016 Aug 05
J1653+3115	...	S/C, 2016 Mar 30
J1655+4551	...	S/C, 2016 Mar 30; S/B, 2016 Aug 05
J1656+3952	L/A	S/C, 2016 Mar 30
J2226+0125	...	S/C, 2016 Feb 04; S/B, 2016 May 30; L/B, 2016 May 31
J2359-1041	...	S/C, 2016 Feb 07; S/B, 2016 May 30; L/B, 2016 Jun 03

Note.^a Roberts et al. (2015a).

(This table is available in machine-readable form.)

Table 3
Typical Angular Resolutions of the Images

Array	Band	Resolution ^a
A	L	1''5
AB	S	2''
B	C	1''5
B	S	2''
B	L	4''
C	S	6''

Note.^a Nominal smallest dimension of the synthesized beam for our snapshot images.

2. Sample Selection

Cheung (2007) created a sample of candidate X-shaped radio sources using the NRAO FIRST survey of radio sources as follows. The key criteria were (1) the fields had to have sufficient dynamic range in the images to be able to see extended low

Table 4
Figure Properties

Source IAU Name	Figure Number	A-array L-band ^a Low, Peak ^b (mJy beam ⁻¹)	B-array C-band ^a Low, Peak ^b (mJy beam ⁻¹)	AB-array S-band Low, Peak ^b (mJy beam ⁻¹)	B-array L-band Low, Peak ^b (mJy beam ⁻¹)	B-array S-band Low, Peak ^b (mJy beam ⁻¹)	C-array S-band Low, Peak ^b (mJy beam ⁻¹)	Source IAU Name
J0001-0033	1-4	0.10, 2.37	0.18, 6.82	0.09, 2.23	0.10, 10.2	J0001-0033
J0033-0149	5-7	0.18, 10.1	0.09, 3.72	0.09, 11.5	J0033-0149
J0036+0048	8-9	0.18, 65.8	0.09, 25.1	...	J0036+0048
J0045+0021	10-13	0.30, 178	0.50, 60.8	...	0.18, 249	0.18, 109	...	J0045+0021
J0049+0059	14-17	0.09, 2.51	0.18, 9.60	0.09, 2.64	0.10, 12.9	J0049+0059
J0113+0106	18-21	0.70, 18	0.18, 12.5	0.09, 4.32	0.14, 16.4	J0113+0106
J0115-0000	22-24	0.25, 15.2	0.09, 4.99	0.14, 15.6	J0115-0000
J0143-0119	25-29	0.20, 44.4	0.09, 34.0	...	0.28, 80.5	0.09, 47.0	0.16, 110	J0143-0119
J0144-0830	30-33	0.09, 1.40	0.20, 7.25	0.09, 1.69	0.16, 5.88	J0144-0830
J0145-0159	34-37	0.20, 2.56	0.25, 9.45	0.09, 3.02	0.20, 18.7	J0145-0159
J0147-0851	38-40	0.18, 33.2	0.09, 14.4	0.16, 30.2	J0147-0851
J0211-0920	41-44	0.10, 2.81	0.18, 10.6	0.09, 2.65	0.13, 14.4	J0211-0920
J0225-0738	45-47	0.20, 51.4	0.09, 18.3	0.18, 49.1	J0225-0738
J0702+5002	48-51	0.22, 5.74	0.18, 28.4	0.07, 4.88	0.09, 21.7	J0702+5002
J0725+5835	52-55	0.22, 4.11	0.18, 10.0	0.07, 2.77	0.09, 8.19	J0725+5835
J0805+4854	56-58	0.18, 11.5	0.10, 4.38	0.06, 5.86	J0805+4854
J0813+4347	59-62	0.14, 9.91	0.18, 22.1	0.07, 9.93	0.09, 17.1	0813+4347
J0821+2922	63-66	0.16, 1.93	0.17, 9.40	0.06, 1.98	0.09, 13.8	J0821+2922
J0836+3125	67-70	0.16, 41.1	0.28, 60.0	0.09, 30.5	0.09, 53.5	J0836+3125
J0838+3253	71-74	0.13, 5.52	0.20, 6.89	0.09, 6.54	0.09, 10.6	J0838+3253
J0845+4031	75-78	0.20, 15.5	0.20, 31.7	0.09, 11.1	0.09, 32.3	J0845+4031
J0846+3956	79-82	0.18, 16.1	0.20, 33.0	0.06, 11.1	0.09, 33.1	J0846+3956
J0859-0433	83-85	0.20, 23.4	0.20, 26.8	0.07, 16.0	...	J0859-0433
J0914+1715	86-89	0.31, 157	0.35, 586	0.13, 160	0.18, 335	J0914+1715
J0917+0523	90-92	0.28, 96.6	0.35, 165	0.14, 74.2	...	J0917+0523
J0924+4233	93-96	0.28, 6.24	0.17, 43.8	0.09, 4.74	0.10, 29.2	J0924+4233
J0941-0143	97-99	0.60, 76.9	0.35, 188	0.14, 68.2	...	J0941-0143
J0941+2147	100-103	0.28, 54	0.25, 79.6	0.09, 39.5	0.13, 56.5	J0941+2147
J0943+2834	104-107	0.20, 62.5	0.50, 142	0.13, 53.7	0.13, 91.3	J0943+2834
J1005+1154	108-110	0.20, 2.72	0.28, 16.8	0.07, 3.57	...	J1005+1154
J1008+0030	111-113	0.20, 66.1	0.35, 75.2	0.08, 75.2	...	J1008+0030
J1015+5944	114-116	0.20, 98.1	0.09, 49.3	0.10, 86.7	J1015+5944
J1040+5056	117-118	0.06, 2.20	0.07, 7.63	J1040+5056
J1043+3131	119-122	0.40, 44.6	0.08, 36.2	0.09, 37.8	0.10, 68.0	J1043+3131
J1049+4422	123-124	0.09, 4.50	0.10, 21.4	J1049+4422
J1054+5521	125-127	0.18, 14.1	0.09, 9.40	0.10, 21.5	J1054+5521
J1055-0707	128-129	0.09, 16.6	0.10, 42.9	J1055-0707
J1102+0250	130-131	0.13, 83.0	0.10, 96.4	J1102+0250
J1111+4050	132	...	0.13, 11.3	J1111+4050
J1114+2632	133-134	0.09, 26.8	0.07, 62.0	J1114+2632
J1120+4354	135-136	0.09, 38.2	0.10, 71.0	J1120+4354
J1128+1919	137-138	0.25, 19.8	0.09, 15.1	...	J1128+1919
J1135-0737	139-141	0.20, 2.00	0.09, 3.86	0.07, 7.39	J1135-0737
J1140+1057	142-143	0.25, 32.3	0.09, 14.0	...	J1140+1057
J1200+6105	144	0.05, 7.61	...	J1200+6105
J1201-0703	145-146	0.10, 8.29	0.10, 19.8	J1201-0703
J1202+4915	147-148	0.15, 7.97	0.05, 7.34	...	J1202+4915
J1206+3812	149-151	0.20, 47.0	0.15, 23.1	0.07, 24.7	...	J1206+3812
J1207+3352	152	0.07, 51.6	...	J1207+3352
J1210-0341	153-155	0.10, 2.95	0.09, 5.28	0.07, 16.5	J1210-0341
J1210+1121	156-157	0.20, 17.3	0.09, 4.57	...	J1210+1121
J1211+4539	158	0.20, 43.6	J1211+4539
J1218+1955	159	0.14, 88.4	...	J1218+1955
J1227-0742	160-162	0.18, 0.86	0.13, 3.12	0.09, 7.47	J1227-0742
J1227+2155	163-164	0.18, 3.74	0.10, 2.91	...	J1227+2155
J1228+2642	165-166	0.08, 4.35	0.10, 5.66	...	J1228+2642
J1232-0717	167-168	0.10, 19.0	0.10, 53.4	J1232-0717
J1247+4646	167	0.07, 3.23	...	J1247+4646
J1253+3435	170-171	0.09, 17.0	0.14, 13.8	...	J1253+3435
J1258+3227	172	0.14, 120	...	J1258+3227
J1309-0012	173-174	...	0.30, 113	0.20, 60.1	...	J1309-0012
J1310+5458	175-176	0.20, 11.3	0.07, 7.72	...	J1310+5458

Table 4
(Continued)

Source IAU Name	Figure Number	A-array L-band ^a Low, Peak ^b (mJy beam ⁻¹)	B-array C-band ^a Low, Peak ^b (mJy beam ⁻¹)	AB-array S-band Low, Peak ^b (mJy beam ⁻¹)	B-array L-band Low, Peak ^b (mJy beam ⁻¹)	B-array S-band Low, Peak ^b (mJy beam ⁻¹)	C-array S-band Low, Peak ^b (mJy beam ⁻¹)	Source IAU Name
J1316+2427	177	0.10, 10.5	...	J1316+2427
J1327-0203	178-179	0.20, 20.9	0.20, 23.6	...	J1327-0203
J1330-0206	180	0.10, 3.34	...	J1330-0206
J1339-0016	181	0.14, 6.48	...	J1339-0016
J1342+2547	182-183	0.30, 76.4	0.09, 29.9	...	J1342+2547
J1345+5233	184-186	0.09, 0.92	...	0.07, 2.47	0.18, 8.74	J1345+5233
J1348+4411	187-189	0.07, 5.96	...	0.06, 4.59	0.07, 24.0	J1348+4411
J1351+5559	190-191	0.04, 4.61	0.07, 17.4	J1351+5559
J1406-0154	192-193	0.30, 57.6	0.09, 24.2	...	J1406-0154
J1406+0657	194	0.20, 71.4	J1406+0657
J1408+0225	195	0.10, 13.9	J1408+0225
J1424+2637	196	0.09, 9.05	...	J1424+2637
J1430+5217	197-199	0.20, 40.2	...	0.08, 12.4	0.14, 80.8	J1430+5217
J1434+5906	200-202	0.15, 47.3	...	0.06, 23.4	0.14, 41.2	J1434+5906
J1444+4147	203-204	0.10, 2.15	0.14, 17.9	J1455+3237
J1455+3237	205	0.06, 1.16	...	J1455+3237
J1456+2542	206	0.11, 1.18	J1456+2542
J1459+2903	207-208	0.20, 8.67	0.10, 10.1	J1459+2903
J1501+0752	209	0.07, 14.0	...	J1501+0752
J1515+0532	210	0.15, 70.3	...	J1515+0532
J1522+4527	211	0.07, 17.3	J1522+4527
J1537+2648	212-213	0.15, 3.57	0.10, 16.8	J1537+2648
J1600+2058	214-216	0.20, 6.89	0.10, 8.72	0.10, 21.3	J1600+2058
J1603+5242	217	0.20, 42.7	J1603+5242
J1606+0000	218-219	0.20, 82.8	0.25, 80.5	...	J1606+0000
J1606+4517	220-221	0.20, 3.22	0.10, 11.1	J1606+4517
J1614+2817	222-223	0.20, 8.07	0.14, 8.55	...	J1614+2817
J1625+2705	224-225	0.70, 2.80	0.20, 41.8	...	J1625+2705
J1653+3115	226	0.40, 74.1	J1653+3115
J1655+4551	227-228	0.10, 5.30	0.14, 16.7	J1655+4551
J1656+3952	229-230	0.20, 8.06	0.07, 20.8	J1656+3952
J2226+0125	231-233	0.28, 10.9	0.09, 4.12	0.20, 8.79	J2226+0125
J2359-1041	234-236	0.25, 12.3	0.13, 11.2	0.14, 18.8	J2359-1041

Notes.^a Roberts et al. (2015a).^b Lowest contour and peak intensity, in mJy beam⁻¹.

(This table is available in machine-readable form.)

surface brightness wings, and (2) sources had to have resolved structures easily discernible with $\sim 5''$ resolution; this meant they had at least $\sim 15''$ major axes. Thus, the FIRST catalog was searched for all those whose peak flux was at least 5 mJy beam⁻¹ at 1.4 GHz and had a major axis size of at least $15''$; there were 1648 sources that met these criteria. Since a defining characteristic of XRGs is off-axis emission, the images were searched by eye for those with suggestions of such structures. Out of the 1648 sources a total of 100 were chosen as promising XRG candidates. The names, coordinates, and redshifts of the sources in the Cheung sample are listed in Table 1. This is by no means an unbiased selection of extragalactic radio sources with off-axis emission, but rather it is a hand-selected list of possible XRGs suitable for detailed observation. Complete details of the properties of the candidate sources are given in a companion paper (Saripalli & Roberts 2017).

3. Observations

We observed 89 of the 100 sources in the Cheung (2007) sample of candidate XRGs from 2016 February 4 through

2017 January 10 using the VLA at L (1.4 GHz) and S bands (3 GHz) and the A, B, and C arrays (one epoch was in the transitional AB-array). Each source was observed in a single snapshot that ranged from about 180 s to about 240 s duration, depending on scheduling constraints. Our goal was to reach the same sensitivity for each source in a given frequency-array combination, and no attempt was made to equalize the dynamic ranges of the images. The integration times were set by the goal of observing as many sources from the sample as possible while still providing adequate sensitivity to see the extended emission.

At S-band we used 16 spectral windows of 128 MHz, each with a net average frequency of about 3 GHz, while at L-band we used 16 spectral windows of 64 MHz width, with an average frequency of between 1.4 and 1.6 GHz, depending on the flagged spectral windows. The spectral windows were each divided into 64 channels. Each data set was edited for interference by the pipeline (see below) and then inspected by hand, with a typical loss of a few of the spectral windows. The log of our observations is given in Table 2. All in all, we had data from both archival VLA data (Roberts et al. 2015a)

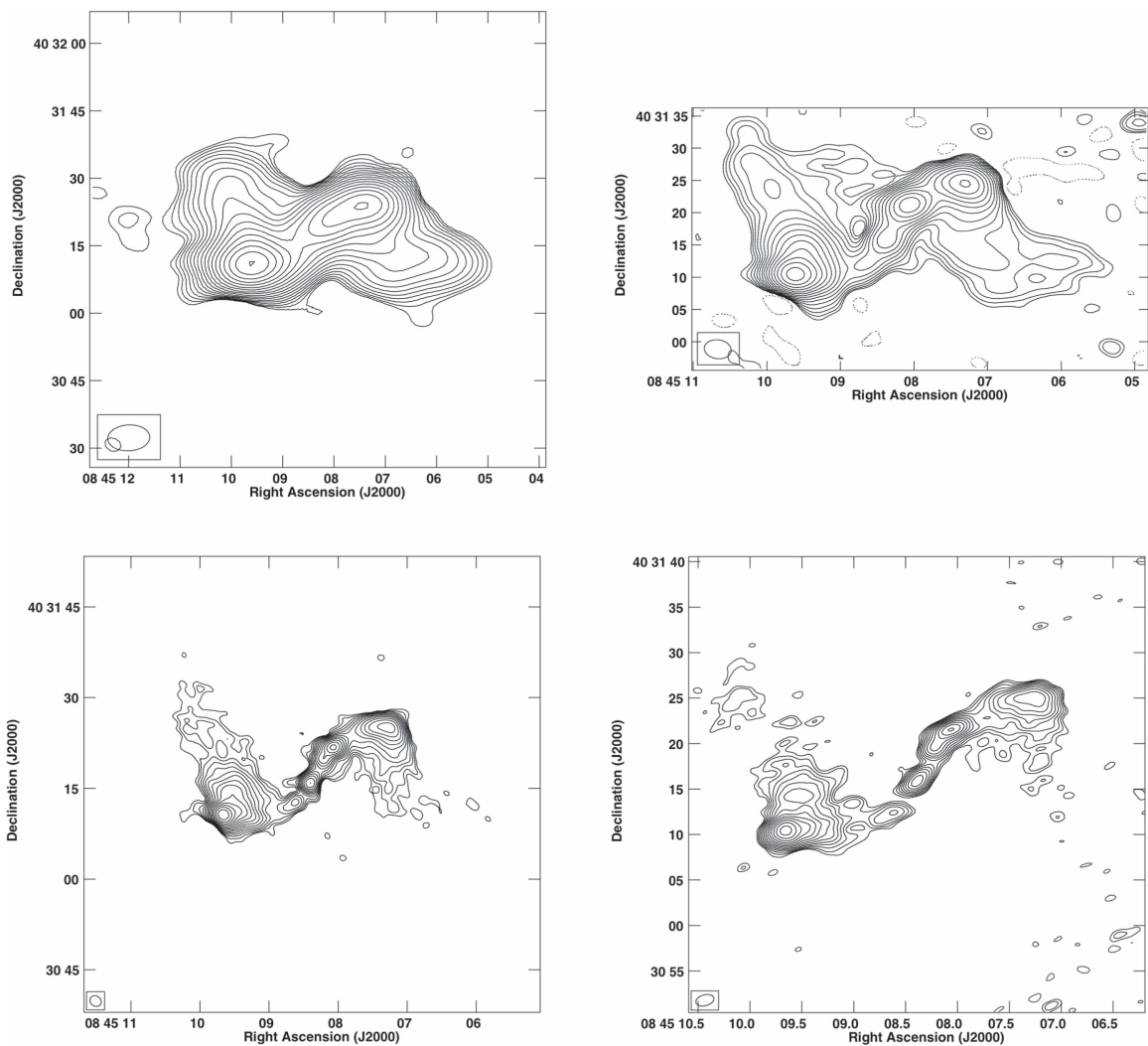


Figure 1. VLA images of J0845+4031 made with four different frequency/array combinations. (top left) S-band C-array; (top right) L-band B-array; (bottom left), S-band B-array; (bottom right) L-band A-array. All of the images and optical overlays are available in the online journal.

and new VLA data on 46 sources, archival data only on 6, new VLA data only on 43, and a total of 5 sources were missed altogether.

Although VLA observations were proposed for the full sample of 99 sources (one source was found to be of head–tail nature based on the archival data in Roberts et al. 2015a) with multiple frequencies and arrays,⁴ we could observe only a subset of sources in each of the arrays and frequencies because of the reduced observing time that was granted and the “C” priority assigned to most of that time. The data were analyzed at Brandeis University. We used our own version of the CASA (McMullin et al. 2007) VLA data calibration pipeline package; this was the standard NRAO VLA pipeline to which we added polarization calibration.⁵

Total intensity, spectral index, and complex polarization images were made of every source–frequency–array combination that we obtained using multi-frequency synthesis (Rao & Cornwell 2011) in CASA. Where possible, the images were

self-calibrated in CASA using a Python script to do the bookkeeping (Harrison 2014).⁶ The angular resolutions of the images depended on the array and frequency and are listed in Table 3. The typical dynamic range of the resulting images was $\sim 100:1$; this was limited by the short integration times and resulting incomplete uv coverage. The quality of each image can be judged from its lowest contour and its peak, as listed in Table 4.

4. The Images

Illustrative examples of the images are shown in Figure 1, where four combinations of array and frequency are used. Radio images for all of the sources are presented in the figure set of Figure 2. In Table 4, we give the lowest contour and peak of each image; in all cases, the contours increase in successive powers of $2^{1/2}$. There is also an optical overlay for each source, presented in the figure set of Figure 3. The overlays are made with the one image of each source that we judged to have the best combination of dynamic range and angular resolution to relate the radio and optical

⁴ The original proposal was for A-array at L-band, B-array at L and S bands, and C-array at S-band for each of the 99 sources.

⁵ The NRAO VLA pipeline now contains polarization calibration.

⁶ The self-calibration script emulates the flow of the Caltech program DIFMAP (Shepherd et al. 1994); it is available from D.H.R.

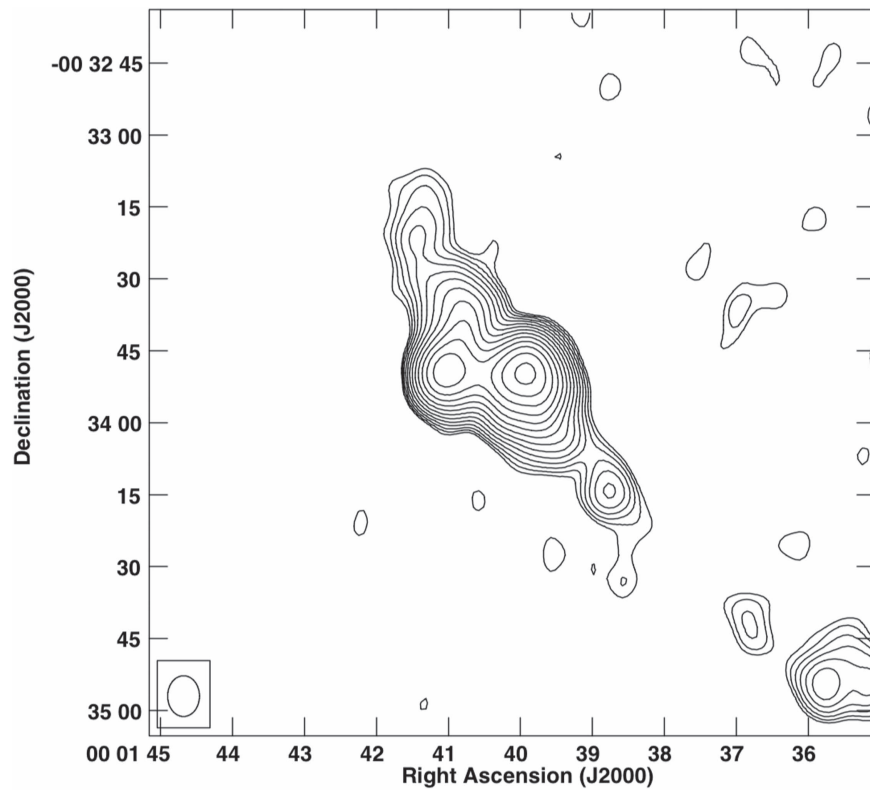


Figure 2. VLA image.
(The complete figure set (236 images) is available.)

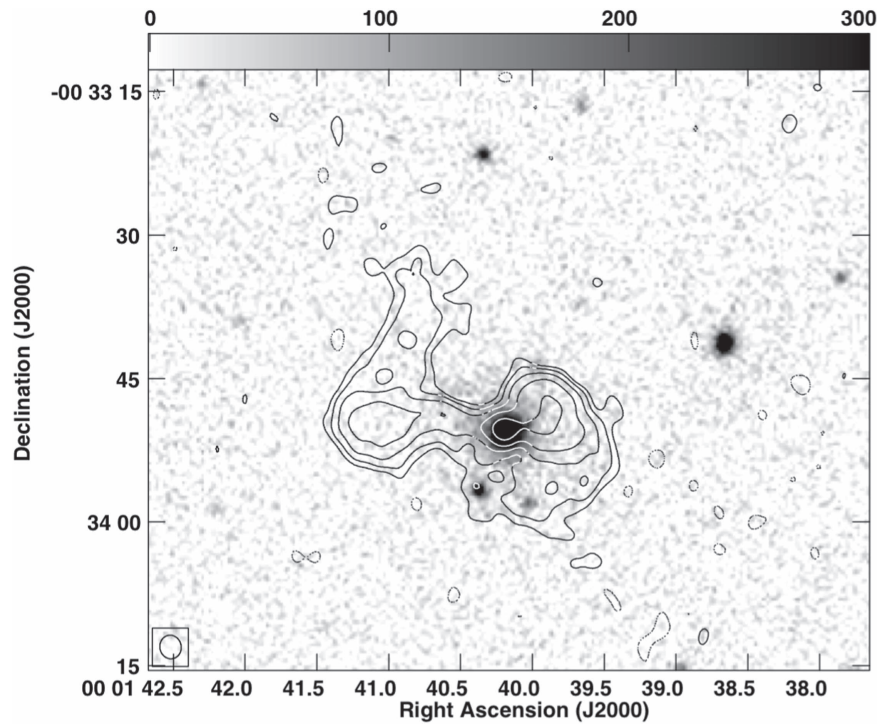


Figure 3. Optical overlay.
(The complete figure set (96 images) is available.)

structures. The overlays were mostly derived from SDSS DR-12 r-band images, and in the nine cases⁷ where these were unavailable, from the USNO Image and Catalog Archive Server (<http://www.usno.navy.mil/USNO/astrometry/optical-IR-prod/icas>).

5. Summary

This is the first in a series of papers in a project aimed at studying a uniformly selected large sample of candidate X-shaped radio sources. In this paper, we present archival and Jansky VLA multi-band multi-array continuum imaging of 95 sources out of a sample of 100 radio sources that were selected by Cheung (2007) as candidate XRGs. The entire set of images, a total of 236 images at a variety of frequencies and in three different VLA arrays, is shown along with an optical overlay for each source. The spectral index and linear polarization information obtained from our observations will be presented and analyzed in further papers in this series.

The paper is intended as a resource base with its full complement of radio images for each source. In a companion paper, we choose a subsample of 87 for thorough study, characterize their morphologies, and present scenarios for their formation (Saripalli & Roberts 2017).

Our multi-band multi-array images have resulted in a revision of source classifications and some of the “XRG candidates” have now been found not to be genuine XRGs, although some have been found to retain genuine XRG morphological characteristics. Details of source classifications, interpretation of structures, and their implications are given in our companion paper.

The National Radio Astronomy Observatory is a facility of the National Science Foundation, operated under cooperative agreement by Associated Universities, Inc. Funding for the Sloan Digital Sky Survey IV has been provided by the Alfred P. Sloan Foundation, the U.S. Department of Energy Office of Science, and the Participating Institutions. SDSS-IV acknowledges support and resources from the Center for High-Performance Computing at the University of Utah. The SDSS web site is www.sdss.org. D.H.R. gratefully acknowledges the

support of the William R. Kenan, Jr. Charitable Trust. We thank Rachel Harrison for her CASA self-calibration script and the anonymous referee for useful comments that led to an improved presentation.

Facilities: VLA (VLA/16A-220, VLA/16B-023, VLA data archive).

Software: CASA (McMullin et al. 2007), AIPS (Bridle & Greisen 1994), DIFMAP (Shepherd et al. 1994).

ORCID iDs

David H. Roberts  <https://orcid.org/0000-0001-5226-4540>
Ravi Subrahmanyan  <https://orcid.org/0000-0001-9913-900X>

References

- Begelman, M. C., Blandford, R. D., & Rees, M. J. 1980, *Natur*, **287**, 307
Bridle, A. H., & Greisen, E. W. 1994, The NRAO AIPS Project-A Summary, AIPS Memo 87 (Charlottesville, VA: NRAO)
Cheung, C. C. 2007, *AJ*, **133**, 2097
Cheung, C. C., Healey, S. E., Landt, H., Verdoes Kleijn, G., & Jordan, A. 2009, *ApJS*, **181**, 548
Deane, R. P., Paragi, Z., Jarvis, M. J., et al. 2014, *Natur*, **511**, 57
Dennett-Thorpe, J., Scheuer, P. A. G., Laing, R. A., et al. 2002, *MNRAS*, **330**, 609
Harrison, R. 2014, Honors thesis in Physics, Brandeis Univ.
Landt, H., Cheung, C. C., & Healey, S. E. 2010, *MNRAS*, **408**, 1103
Leahy, J. P., & Parma, P. 1992, in Extragalactic Radio Sources. From Beams to Jets, ed. J. Roland et al. (Cambridge: Cambridge Univ. Press), 307
Leahy, J. P., & Williams, A. G. 1984, *MNRAS*, **210**, 929
McMullin, J. P., Waters, B., Schiebel, D., Young, W., & Golap, K. 2007, in ASP Conf. Ser. 376, Astronomical Data Analysis Software and Systems XVI, ed. R. A. Shaw, F. Hill, & D. J. Bell (San Francisco, CA: ASP), 127
Merritt, D., & Ekers, R. D. 2002, *Sci*, **297**, 1310
Rao, U., & Cornwell, T. 2011, *A&A*, **532**, 71
Roberts, D. H., Cohen, J. P., Liu, J., Saripalli, L., & Subrahmanyan, R. 2015a, *ApJS*, **220**, 7
Roberts, D. H., Saripalli, L., & Subrahmanyan, R. 2015b, *ApJL*, **810**, L6
Saripalli, L., & Roberts, D. H. 2017, *ApJ*, **852**, 48
Shannon, R. M., Ravi, V., Coles, W. A., et al. 2013, *Sci*, **342**, 334
Shannon, R. M., Ravi, V., Lentati, L. T., et al. 2015, *Sci*, **349**, 1522
Shepherd, M. C., Pearson, T. J., & Taylor, G. B. 1994, *BAAS*, **26**, 987

⁷ The overlays that use USNO images are for J0702+5002, J0725+5835, J0859-0433, J1055-0707, J1135-0737, J1201-0703, J1227-0742, J1232-0717, and J1515-0532.